J Mater Sci (2009) 44:1006–1015
DOI 10.1007/s10853-008-3222-9

Application of the work of indentation approach for the characterization of aluminium 2024-T351 and Al cladding by nanoindentation

M. K. Khan · S. V. Hainsworth · M. E. Fitzpatrick · L. Edwards

Received: 4 August 2008 / Accepted: 22 December 2008 / Published online: 13 January 2009

Abstract Nanoindentation has been used to characterize the mechanical properties of aerospace-grade Al2024-T351 with and without a clad layer of pure aluminium. The clad layer is introduced by means of a roll-bonding process which can cause significant work-hardening of the material in the clad layer. The hardness and Young's modulus of the pure aluminium and the Al2024 have been determined by a number of methods, including the traditional Oliver and Pharr method, and a number of other methods, including direct measurement of the indentation by atomic force microscopy, and evaluation of the work of indentation. The Oliver and Pharr method was found to underestimate the area of contact as it did not include the area of piled-up material around the indentation periphery. This gave a corresponding overestimation of both hardness and modulus. The area of the indentation measured by atomic force microscopy was similarly found to underestimate the contact area owing to relaxation of material around the indent between indentation and imaging. The work of indentation approach was found to give good agreement between the hardness calculated by nanoindentation and those found in the literature.

M. K. Khan · M. E. Fitzpatrick (✉) · L. Edwards
Materials Engineering, The Open University,
Milton Keynes MK7 6AA, UK
e-mail: m.e.fitzpatrick@open.ac.uk

S. V. Hainsworth
Department of Engineering, University of Leicester,
Leicester LE1 7RH, UK

Present Address:
L. Edwards
Institute of Materials Engineering, ANSTO, PMB1, Menai,
NSW 2234, Australia

Introduction

The use of high-strength and low-weight aluminium alloy parts is widespread in aerospace structural applications. The use of aluminium alloys leads to an overall reduced weight and, thus, to reduced fuel consumption. Alloy 2024-T351 plate is used in fuselage and wing structural areas where stiffness, fatigue performance and good strength are required. Al-cladding, where a commercially pure aluminium cladding is roll-bonded to the alloy, is used extensively to provide additional corrosion resistance to the material.

The overall aim of the present study is to apply instrumented indentation to the study of localized residual stresses in aerospace aluminium materials. A precursor to this goal is the ability to accurately characterize the mechanical properties and indentation response of the material with and without cladding. In this article we focus on the characterization of the elastic response and hardness of the aluminium alloys. Nanoindentation has traditionally been developed and applied to hard ceramic materials and coatings, and hence the existing analysis methods are not optimized for the study of relatively soft materials such as most engineering alloys. To our knowledge, this is the first study to focus on the application of nanoindentation to aluminium for aerospace applications, and the ability to use the technique for these materials is an important development for research on residual stress and damage mechanisms in these materials.

Depth-sensing indentation allows the determination of mechanical properties at very low loads. An indenter of known geometry is driven into the material surface by applying a known load, and the load–displacement data is analyzed typically using the Oliver–Pharr (O–P) model [1]. As the indenter is driven into the material, both elastic and plastic deformation processes occur, producing a hardness impression that corresponds to the shape of the indenter.

It is well known that the ratio of elastic modulus to yield strength, E/Y, and the strain hardening behaviour of materials influence the amount of material pileup around indentations, and that, in particular, nanoindentation hardness and modulus calculations can be critically affected by the extent of the pileup [2–11]. As aluminium has relatively low hardness and stiffness, pileup around the indenter is to be expected, even at small indentation depths. Hence, the actual contact area includes the area contained in the pileup. This additional area in the pileup can contribute significantly to the load-bearing capacity of the contact. Significant pileup is typically observed along the sides of indents in aluminium. As a result, the area of contact calculated from the O–P model is underestimated which results in an overestimate of the calculated hardness and modulus [2, 4, 9, 12].

Atomic force microscopy (AFM) can be applied to measure the 'true' area of the indentation [2, 8, 9]. The measurement of hardness using atomic force microscopy is the method that is most directly comparable to traditional Vickers hardness testing, as it uses direct measurement of the residual area of the indentation. However, in itself, measurement of the indentation area by atomic force microscopy is not straightforward as the material often relaxes between indentation and scanning with AFM, so AFM measured values of residual depth are less than those measured by nanoindentation [7] and consequently provide lower values of hardness. Additionally sources of error are that tip convolution effects can lead to errors in the estimation of the area using the O–P model, and that the area of the indentation itself cannot always be clearly defined from AFM imaging.

A work of indentation approach can also be used for estimation of the hardness from nanoindentation [11, 13–16]. In this method, the elastic, plastic or total work of indentation is calculated from the nanoindentation load–displacement curve and the maximum applied load without the need to calculate indent area or indentation volume. This method is outlined in greater detail below.

In this article we compare the applicability of the Oliver and Pharr method, the Oliver and Pharr method with area correction from measuring the pileup around indentations, and the work of indentation approaches, for measuring the hardness of the Al-cladding and Al2024-T351. The results suggest that the work of indentation approach affords several improvements in hardness measurement and interpretation, particularly for ultra-low loads in these materials.

Theoretical background

Oliver and Pharr method

In depth-sensing indentation testing, an indenter penetrates into the surface of a material. The total penetration depth is the summation of the elastic and plastic deformations occurring at the indenter tip. The plastic depth corresponds to the contact depth, which is used to determine the contact area. During the unloading stage, only the elastic portion of the displacement is recovered, which effectively allows separation of the elastic properties of the material from the plastic. A schematic representation of indentation load P versus displacement h obtained during one full cycle of loading and unloading is presented in Fig. 1a.

One of the more commonly used methods for analyzing nanoindentation load–displacement data is that of Oliver and Pharr [1]. In the Oliver–Pharr method, hardness and elastic modulus are determined from indentation data obtained during one complete cycle of loading and unloading.

According to elastic contact theory [17], the fundamental relations from which hardness and elastic modulus can be determined are:

$$H = \frac{P}{A} \tag{1}$$

where H is hardness, P is the load and A is the projected contact area at that load. The O–P method uses the contact area at maximum load to calculate the material's hardness.

A modified form of Sneddon's relationship is used to calculate the reduced modulus of the material. This is given by

$$E_r = \frac{\sqrt{\pi}}{2\beta}\frac{S}{\sqrt{A}} \tag{2}$$

where E_r is the reduced elastic modulus, S is stiffness and β is a constant that depends on the geometry of the indenter. For triangular cross sections like the Berkovich and cube-corner indenters, $\beta = 1.034$. The reduced modulus, E_r is used to account for the fact that elastic displacements occur in both the indenter and the sample. The elastic modulus of the test material, E_s, is calculated from E_r using:

$$\frac{1}{E_r} = \frac{1-\nu_i^2}{E_i} + \frac{1-\nu_s^2}{E_s} \tag{3}$$

where E_s and ν_s are the elastic modulus and Poisson's ratio for the test material; and E_i and ν_i are the elastic modulus and Poisson's ratio for the indenter. For diamond, the elastic constants $E_i = 1140$ GPa and $\nu_i = 0.07$ are often used.

In the O–P method, the unloading curve is fitted to the power-law relation

$$P = B(h - h_f)^m \tag{4}$$

where P is the indentation load, h is the displacement, B and m are empirically-determined fitting parameters, and h_f is the final displacement after complete unloading. The geometry of a typical indentation is shown in Fig. 1b.

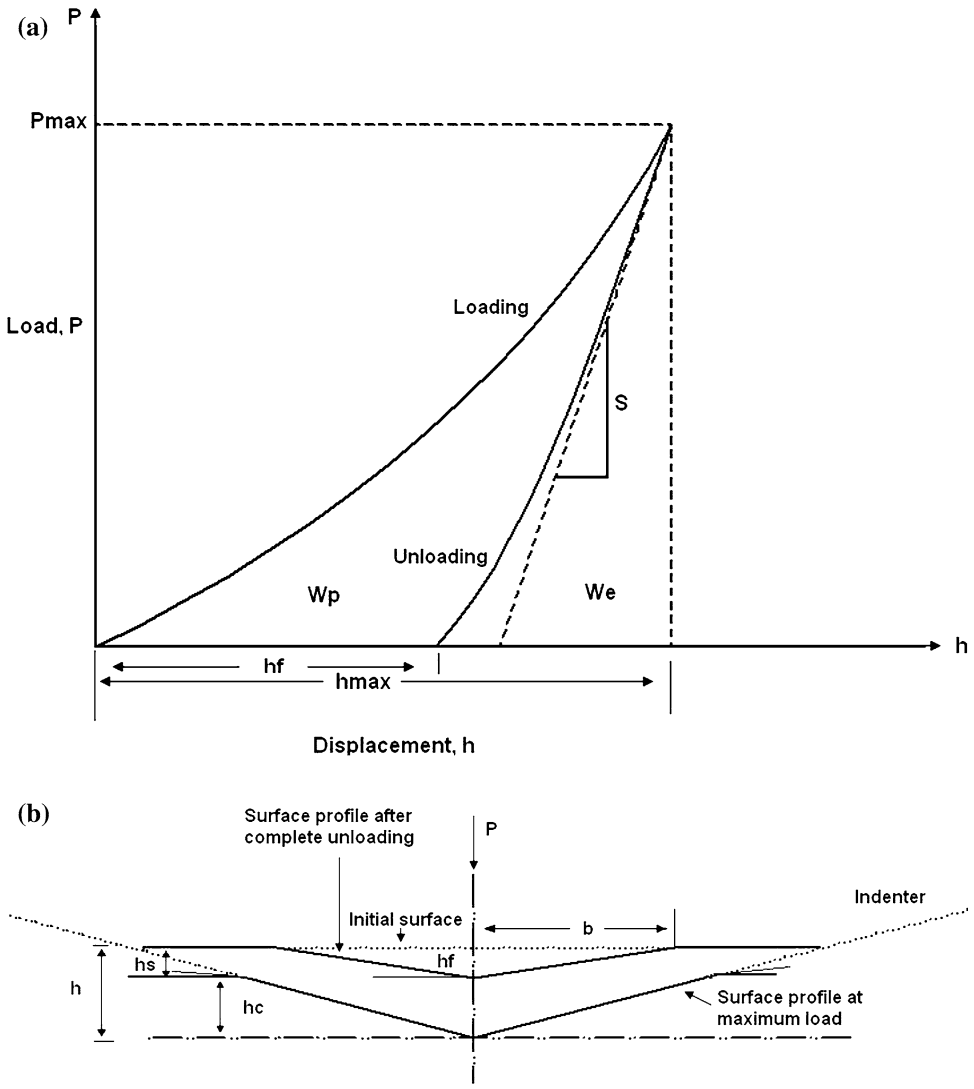

Fig. 1 **a** A schematic load–displacement curve for nanoindentation into an elastic-plastic material. **b** Schematic showing the surface profile of a typical indentation before and after loading

The depth along which contact is made between the indenter and the specimen, h_c, can be estimated from the load–displacement data using:

$$h_c = h_{max} - \varepsilon \frac{P_{max}}{S} \tag{5}$$

where h_{max} is the maximum depth of penetration at P_{max}, the peak indentation load, and ε is a constant which depends on the geometry of the indenter: for a Berkovich Indenter $\varepsilon = 0.75$.

Once the parameters B and m are obtained by curve fitting, the initial unloading stiffness S can be established by differentiating Eq. 4 at the maximum depth of penetration, $h = h_{max}$:

$$S = \left(\frac{dP}{dh}\right)_{h=h_{max}} = mB(h_{max} - h_f)^{m-1} \tag{6}$$

With these basic measurements, the projected contact area of the hardness impression, A, is derived by evaluating an empirically determined indenter shape function at the contact depth, h_c; that is, $A = f(h_c)$. The indenter's tip shape function needs to be accurately determined by calibration of the tip geometry at low penetration depths. To a first approximation, the equation $A = 24.56\, h_c^2$ relates the cross-sectional area of the indenter to the contact depth although calibration of the indenter shape is required to find the area at shallow indentation depths. Finally, the hardness, H, and reduced elastic modulus, E_r, are derived from Eqs. 1 and 2.

One of the problems of the Oliver and Pharr approach is that it can markedly underestimate the true area of contact in cases where significant pileup occurs. In these cases, the true contact area A can be obtained by combining the results of the Oliver–Pharr method A_{O-P} with a correction which takes into consideration practical measurement of the pile-up area A_{PU}:

$$A = A_{O-P} + A_{PU} \tag{7}$$

This approach has been used by a number of workers including Beegan et al. [3, 7], Saha and Nix [9] and Kese

[2, 5, 8]. Beegan et al. [3, 7] and Saha and Nix [9] calculated the area of the pileup by considering the pileup as forming an arc of a certain radius; whilst Kese [2, 5, 8] assumed pileup to be a semi-ellipse with its major axis corresponding to one side of the indent triangle, and the minor axis being the horizontal distance from the vertex of the triangle to the peak height of the pileup. The area of pileup is typically obtained from measurements of the pile-up area from scanning electron micrographs or atomic force microscopy images of the indentations.

Work of indentation approach

In nanoindentation experiments, the work of indentation can be calculated conveniently from the areas bounded by the loading and unloading curves (Fig. 1a). The area under the loading curve gives the total work W done by the loading device during indentation. The elastic contribution to the total work, W_e, can be deduced from the area under the unloading curve, and the energy absorbed by plastic deformation is then the difference between these:

$$W_P = W_t - W_e \tag{8}$$

Stillwell and Tabor [17] first applied this method to determine hardness. This technique equates the conventional hardness—of maximum applied load divided by the residual area of indent impression—to the plastic work divided by the volume of the indent:

$$\frac{\text{Load}}{\text{Plastic area}} = \frac{\text{Plastic work}}{\text{Plastic volume}} \tag{9}$$

The area under the load–penetration curve represents the total work W_t, given by:

$$W_t = \int_0^{h_{max}} P\,dh \tag{10}$$

For indentation, Kick's Law is given by $P = Ch^2$. Kick's law assumes that the material does not exhibit indentation size effects and that hardness is constant with load. Substituting for P in (15) gives:

$$W_t = \int_0^{h_{max}} Ch^2\,dh = \frac{Ch_{max}^3}{3}\frac{P_{max}h_{max}}{3} \tag{11}$$

Now according to Tuck et al. [13]:

$$H = kP/h^2 \tag{12}$$

where k is a constant which takes into account the indenter geometry and the choice of hardness definition; its value is 0.0408 for a Berkovich indenter.

Rearranging Eq. 12 gives:

$$P = \frac{Hh^2}{k} \tag{13}$$

and

$$h = \sqrt{\frac{Pk}{H}} \tag{14}$$

and Eq. 10 thus becomes:

$$W_t = \int_0^{h_{max}} \frac{Hh^2}{k}\,dh = \frac{Hh_{max}^3}{3k} \tag{15}$$

If we now substitute h from (19) this gives:

$$H = \frac{kP^3}{9W_t^2} \tag{16}$$

If we consider hardness as a function of only plastic deformation then we need to use the plastic work during the indentation process and thus Eq. 16 becomes:

$$H = \frac{kP^3}{9W_p^2} \tag{17}$$

Hence using Eqs. 16 and 17, the hardness of a material can be obtained from the work of indentation technique.

Tuck et al. [13, 16] and Beegan et al. [11] applied this technique to ductile materials where owing to the softness of the material, significant pileup occurs at the edges of indentations.

In this article, we use the work of indentation approach to calculate the hardness using both the total work (i.e. $W_e + W_p$) and the plastic work W_p alone.

Materials and experimental methods

The materials used in this study were in the form of cold rolled plate of Al2024-T351 of 2 mm thickness, with an aluminium cladding of 80 μm on both faces. For one sample, the aluminium cladding was removed by chemical milling.

The grain size of the Al2024-T351 was determined by quantitative metallography and electron back scattered diffraction (EBSD), and was found to be 20 μm. The grains were equiaxed and showed a random orientation. The grain size of the Al-clad was not measured directly here owing to the difficulties of preparing metallographic samples of such a thin, soft layer which is difficult to etch, but previous work has shown it to be in the range 30–70 μm.

Surface scanning of both materials was performed using atomic force microscopy (AFM), after surface polishing of samples to a 1 μm finish. A DME Dual Scope C-21 AFM was used to perform observations of the indentations and particularly of the pileup at their periphery. Measured

surface profiles are shown in Fig. 2a and b which shows the topography of the clad and unclad layers, respectively. The surface roughness of the clad layer was greater than the surface roughness of the Al2024. The Al2024 has a very smooth surface owing to the chemical milling process used to remove the cladding.

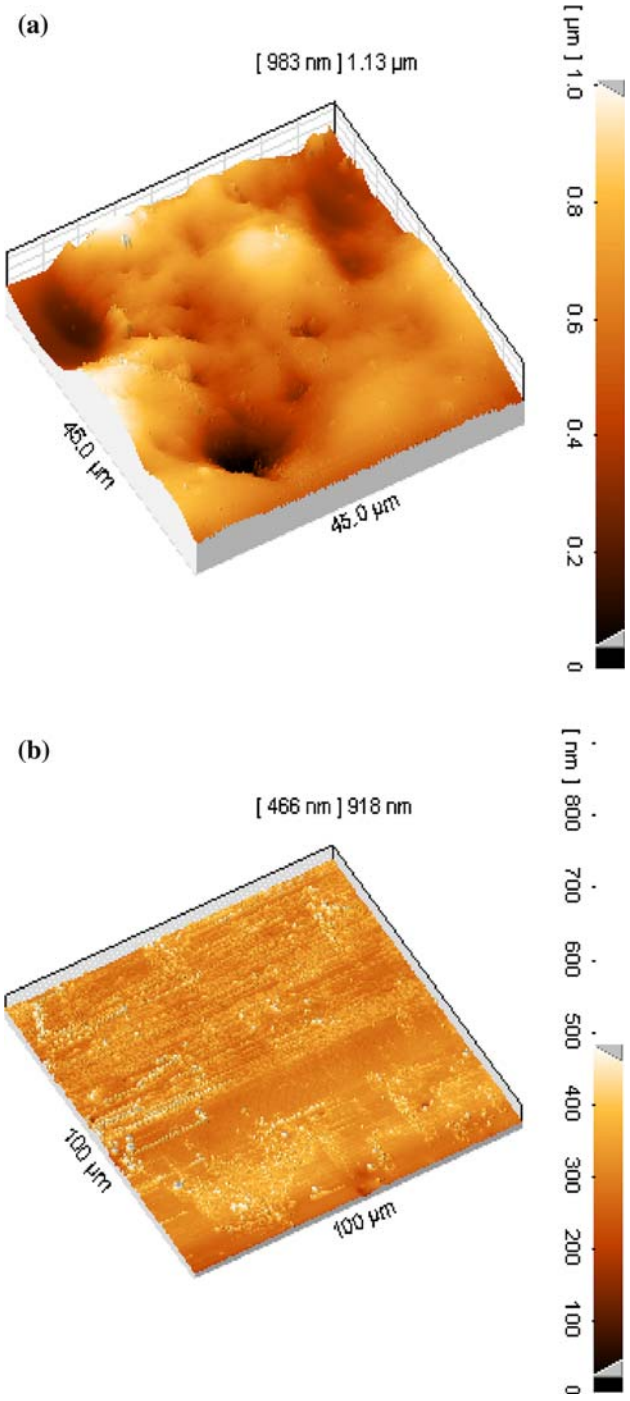

Fig. 2 Surface profiles using AFM for the **a** clad and **b** unclad 2024 material showing that the clad layer has greater surface roughness than the unclad 2024

The mechanical properties of the Al-clad and substrate Al2024-T351 were characterized using an MTS Nano-indenter XP system with a Berkovich indenter tip. The instrument was operated in basic hardness load–displacement mode which simply records load, displacement and time, and in contact stiffness mode (CSM) where an oscillating force with a force amplitude generally several orders of magnitude smaller than the nominal load is applied at the same time as the indenter load. The CSM allows the contact stiffness to be obtained at all points on the load–displacement curve, and hardness and modulus can be obtained as function of penetration depth. Indentations were made using a constant nominal strain rate ($\dot{P}/P$) of 0.05 s^{-1} and the drift rate before testing was required to be <0.05 nm s^{-1}. Twenty-five indents were made at each depth in an array of 5 × 5 with spacing of 100 µm in both axes. The depths of the indentations ranged from 200 to 2400 nm in steps of 200 nm. These indentation depths correspond to applied loads from 1 to 70 mN for the Al-cladding, and 2.5 to 220 mN for the Al 2024-T351.

Results and discussion

Characterization using the Oliver and Pharr model

When the indentation data was analyzed using the Oliver–Pharr model, values of both the hardness and modulus were found to be overestimated. The hardness and modulus obtained from O–P for the Al cladding were calculated as 0.48–0.56 GPa and 73–75 GPa, respectively; and for the Al2024-T351, 1.64–1.80 GPa and 77–80 GPa, respectively. Typical literature values of hardness and elastic modulus for hard aluminium (rolled or stretched) are 0.37–0.50 GPa and 69 GPa, respectively, and for Al 2024-T351 are 1.44–1.7 GPa and 73 GPa, respectively. These hardness values are for bulk materials, measured by traditional macro-Vickers indentation tests which are unsuited to measure the relatively thin clad layers here. The hardness values for the Al-cladding, measured by nanoindentation, were thus 25% higher than the literature values, whilst the values for Al 2024-T351 were 15% higher. This overestimation, for both the hardness and the modulus, can be attributed to the pileup around the indentations, which is not accounted for in the analysis. Pile-up effects on macro-indentation measurement are less significant than for nanoindentation as pileup occurs mainly around the edges of the indentations, and macro-indentation measurement is based upon evaluation of the size of the indentation diagonals. Therefore, it is more critical for the accuracy of nanoindentation measurement that pile-up effects are taken into account.

Pile-up formation

Since aluminium has relatively low hardness and modulus, pileup around the indenter is to be expected, even at small indentation depths. This is shown in Fig. 3 which shows a scanning electron microscope image of an indentation in Al 2024. There is clear evidence of pileup around the indentation periphery. Figure 4a shows an AFM height profile from the corner of an indentation through the midpoint of the edge of the indentation (Fig. 4b). Pileup on the edge can be clearly seen in the AFM trace. Hence, the actual contact area includes the area contained in the pileup, and because significant pileup occurred at all the indentations its influence on the determination of the true contact area cannot be ignored. The additional contact area associated with the pileup can contribute significantly to the load-bearing capacity of the contact.

The area of pileup forms a semi-ellipse. Thus, following Kese [2, 5, 8], the area of pileup was calculated from the measurements as illustrated in Fig. 5. The point T on Fig. 5 marks the perimeter of the contact when viewed in profile; its horizontal displacement from the edge L of the nano-indentation is measured to be a_i ($i = 1, 2, 3$ for the three pile-up lobes).

The pile-up contact perimeter is obtained by projecting a semi-ellipse of major axis b and minor axis a_i, so that the length of the side of the projected triangular area is b, calculated at the contact depth h_c, whilst a_i is measured on the indent profile image as the horizontal distance of the pile-up contact perimeter T from the edge L of the indentation (see Fig. 5).

The triangular indentation area can be calculated as:

$$A_{O-P} = 0.433b^2 \tag{18}$$

The indentation area as a function of contact depth for a perfect Berkovich tip is given by:

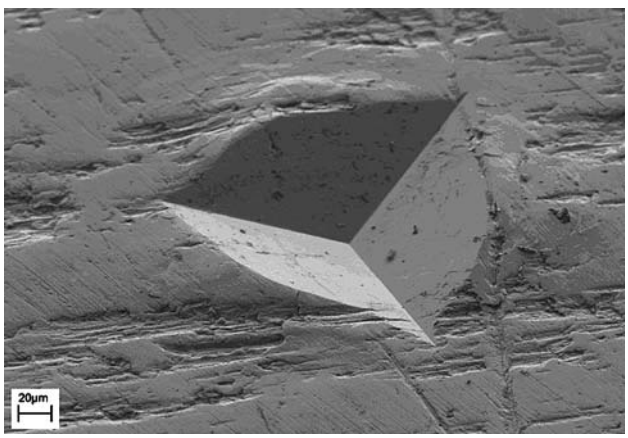

Fig. 3 SEM image of an indentation in Al2024 showing extensive pileup around the periphery of the indentation

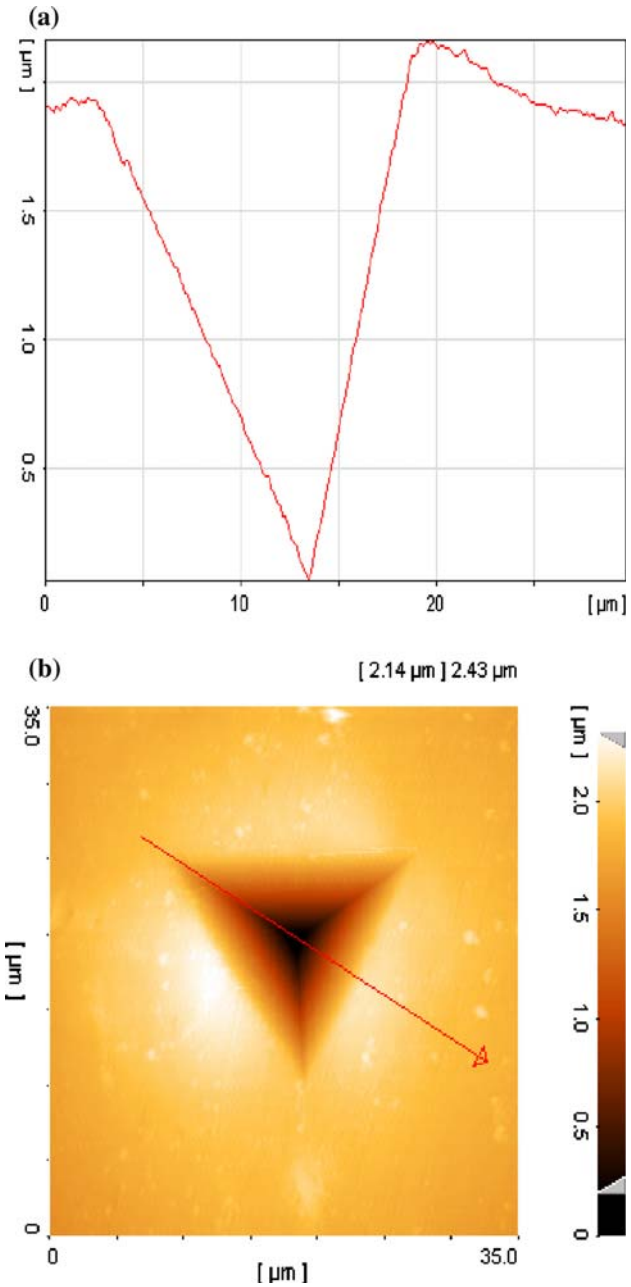

Fig. 4 **a** Height profile through an indentation (from one corner to the midpoint of the opposite edge) showing significant pile up on the indentation edge, **b** The scan across the indent from which the data in (**a**) was obtained

$$A_c = 24.56h_c^2 \tag{19}$$

From Eqs. 18 and 19:

$$b = 7.531h_c \tag{20}$$

The total pile-up area of the three semi-elliptical lobes around each side of the indent triangle, which may differ from each other, will be:

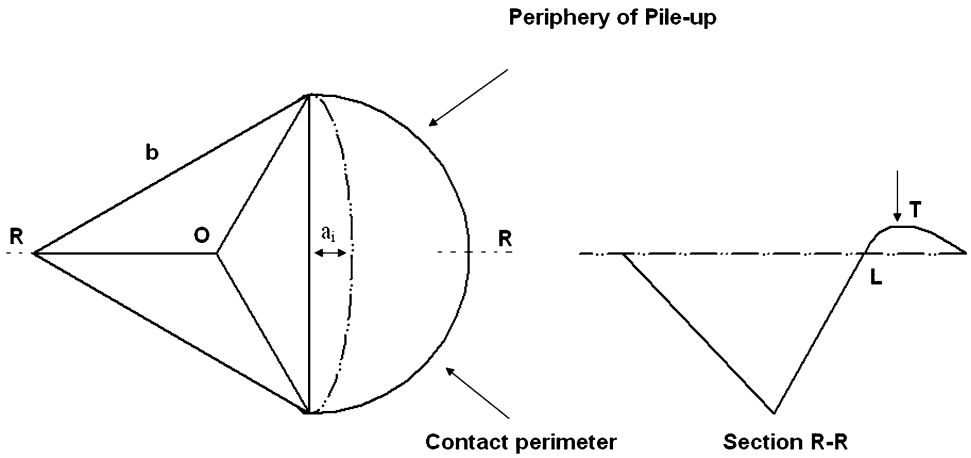

Fig. 5 Schematic showing the pile-up profile around the periphery of an indentation (after Kese [2, 5, 8])

$$A_{PU} = \frac{\pi b}{4}\sum a_i \tag{21}$$

a_i can be obtained by measuring the horizontal displacement around each of the three sides of the indent.

$$A_{PU} = 5.913 h_c(a_1 + a_2 + a_3) \tag{22}$$

The total indentation area A can be calculated by adding this pile-up area with the area determined from Eq. 18.

The amount of pile-up area, in terms of the percentage of the triangular area of indentation calculated from the Oliver–Pharr Model, is shown in Fig. 6. The pileup was measured for indentations made to different penetration depths and found to increase with penetration depth for both Al2024-T351 and the cladding; but for the Al-cladding, owing to its higher E/Y ratio, more pileup was observed at indentation depths of 1 μm or greater.

The E/Y ratios for both Al-cladding and Al2024-T351 are given in Table 1. It can be seen that the E/Y ratio is higher for Al2024 than the Al-cladding. If $E/Y \rightarrow 0$, contact is strictly elastic and dominated by sink-in; as $E/Y \rightarrow \infty$, there is predominantly plastic deformation, and extensive pileup occurs. The differences in the percentage pileup seen in Fig. 6 can thus be accounted for by the higher E/Y ratio of the Al-cladding.

A tensile test was performed on Al2024-T351 to determine its strain-hardening exponent. This was calculated to be 0.13, which is small, and this combined with the relatively high E/Y ratio would predict that significant pileup would be expected (as is observed here). It was not possible to measure the strain-hardening exponent of the Al-cladding. It is probably similar to that measured for the Al2024 based on the fact that the hardness of the roll-clad

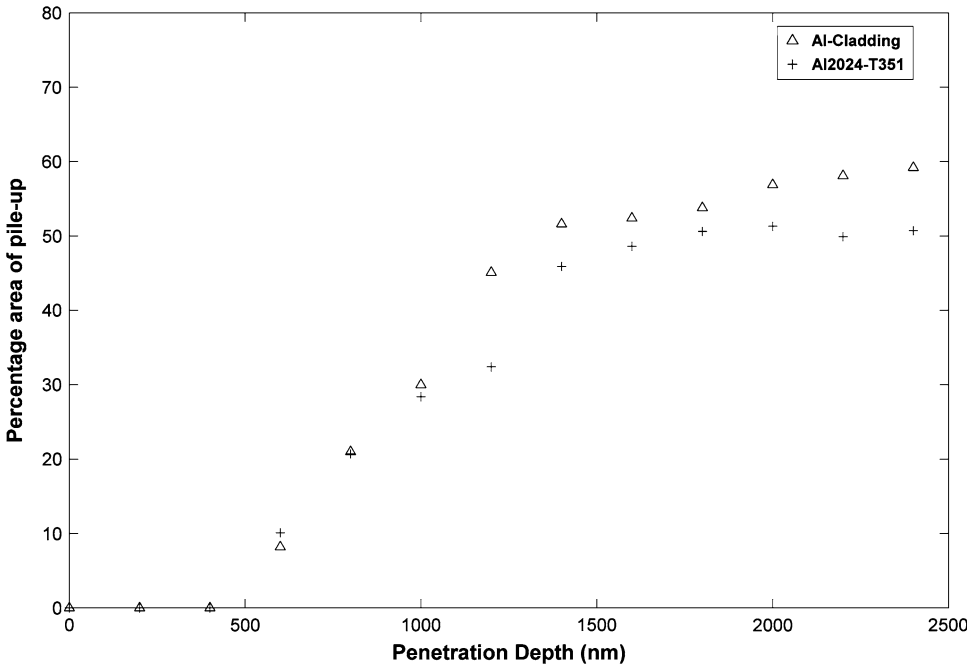

Fig. 6 Percentage area of pile-up for Al-cladding and Al 2024-T351 at different indentation depths. As the indentation depth increases, the contribution of the pile-up to the load bearing capacity of the indentation increases significantly, particularly for the Al-cladding which has a higher E/Y ratio

Table 1 Mechanical property data for Al-Clad and Al2024-T351

Material	E/GPa	σ_y/MPa	Hardness/GPa	E/σ_y
Al-Cladding	69	110	0.45	627
Al 2024-T351	73	360	1.75	203

aluminium is high compared to annealed pure aluminium: significant work-hardening will already have occurred during roll-bonding.

Difference in elastic recovery of Al-Clad and Al2024-T351

The Al-clad material has a much lower hardness than the Al2024-T351. Nanoindentation tests at the same load give a greater indentation depth in the Al-clad compared to Al2024-T351, as shown in Fig. 7. The Al-cladding shows very little elastic recovery of the displacement on unloading. The percentage elastic recovery W_e for the Al-cladding is only 3–4% of the total work W_t, as compared to Al2024-T351 for which the elastic recovery is 10–12%.

Hardness calculated by work of indentation approach

Equations 16 and 17 were used to calculate hardness from the total work and plastic work approaches. The main advantage of these techniques is that there is no need to calculate the area of the indentation, which thus removes the difficulties caused by underestimating the contact area.

The values of hardness as a function of penetration depth for the four different methods of calculation are shown in Fig. 8 for the Al-cladding and in Fig. 9 for the Al2024-T351.

Figure 8 shows that three methods—the O–P model, the total work and plastic work methods—result in hardness values that are very close to each other and the quoted literature values of hardness for the Al-Clad. The hardness values obtained using correction for the area from the AFM measured areas are well below the other three methods [7, 13] (apart from the indentations to displacements of 200 and 400 nm where the O–P and AFM values were found to be equal as no pileup was observed at these depths). As we have discussed above, the AFM measured residual depths were less than the nanoindentation measured depths owing to relaxation of the material between indentation and AFM scanning, and tip convolution effects. AFM is also less accurate when estimating distances in the z-direction.

If we consider the hardness values calculated from the work of indentation methods, at low penetration depths (200 and 400 nm) the hardness calculated from plastic work gives the highest value of hardness, followed by the O–P method and then the hardness calculated from the total work. No pileup was measured on these indentations using the AFM, and the AFM calculated hardness values and hardness values from the O–P method are coincident. At larger penetration depths, the AFM corrected hardness values are low as discussed above whilst the three other methods show very little differences in the values obtained. Of the methods used, the hardness calculated from the total work using the work of indentation gave values of hardness very close to quoted literature values of hardness in the range of 0.45–0.52 GPa. It should be noted that the hardness values calculated from the work of indentation

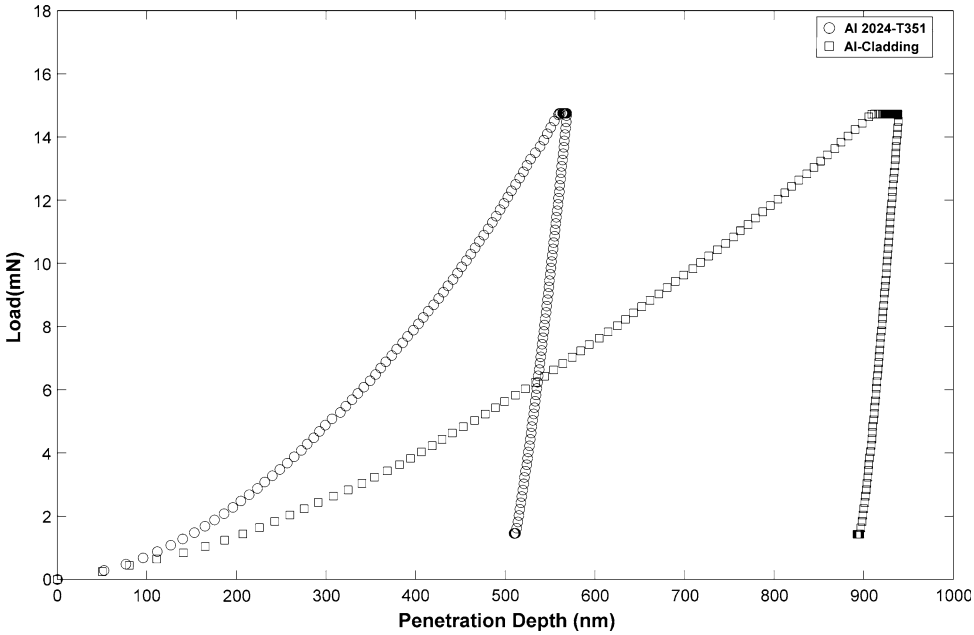

Fig. 7 Load–displacement traces for the Al-clad and Al2024 for a peak load of 15 mN

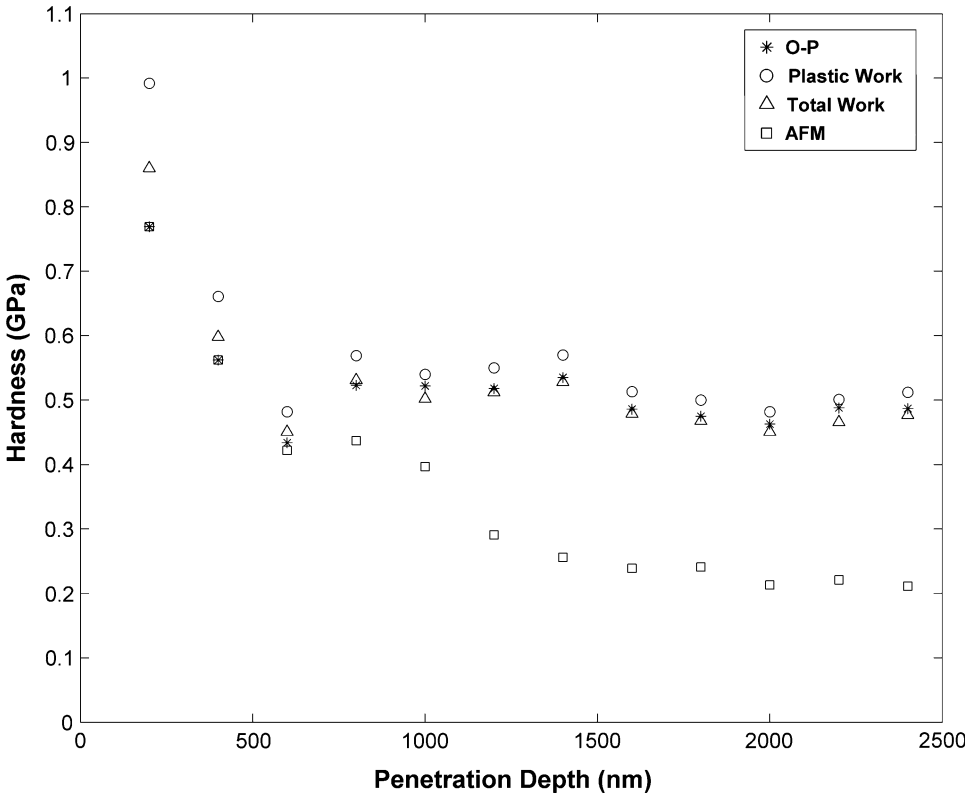

Fig. 8 Hardness calculated using the four different methods for the Al-Clad

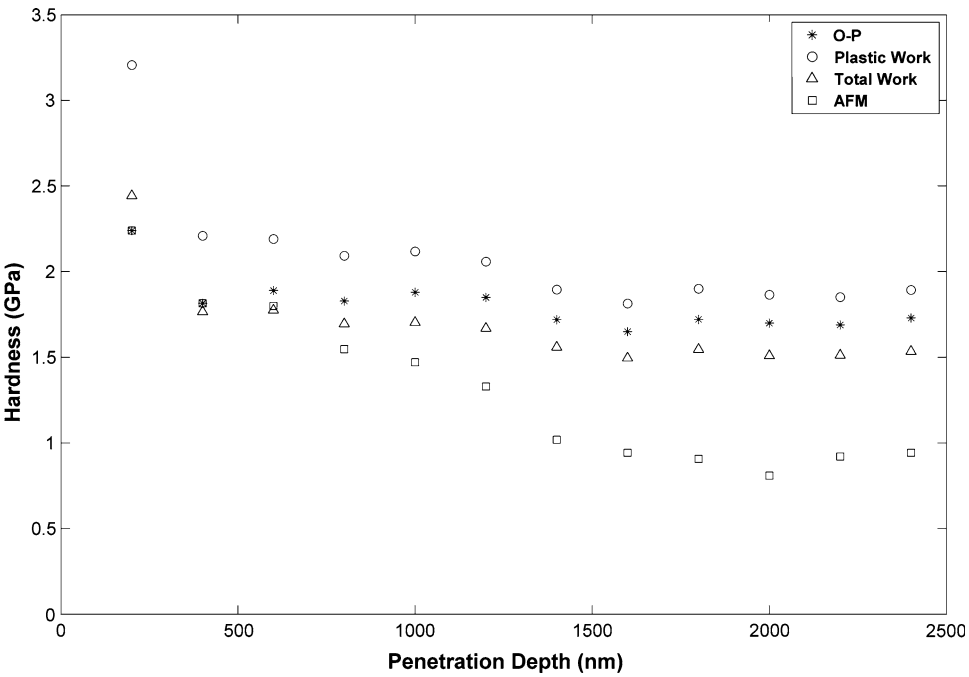

Fig. 9 Hardness calculated using the four different methods for the Al-2024

approach rise more steeply at lower penetration depths than the hardness values calculated by the O–P method. This is likely to be because the method of Tuck et al. [13] makes no allowance for changes in tip geometry at lower indentation depths, where the tip geometry can significantly influence the calculated values, whilst tip geometry effects are allowed for in the O–P calculations.

Figure 9 shows that the hardness values for the Al2024-T351 calculated from the O–P model, and work of indentation using the total work and plastic work approaches, are

again close to each other, as well as to the literature values of the hardness for Al2024-T351. The absolute difference in the values of the hardness calculated by these three methods is greater than for the Al-Clad which corresponds to findings by other researchers [3, 7, 11, 13], and can be attributed to the higher hardness of the Al2024 (the overall percentage spread is similar). The hardness values calculated using the plastic work of indentation are again highest at around 1.81–2.2 GPa, and the O–P model values are also higher than those hardness values calculated using the total work of indentation. The greater differences between the total work of indentation approach and the plastic indentation approach are to be expected owing to the greater elastic recovery for indentations into Al2024. Hardness values calculated from the total work values of indentation were found to be very close to literature values of hardness in the range of 1.51–1.76 GPa.

Thus, for a soft material such as the Al-cladding, where very little elastic recovery of the indentation occurs, both the total work and plastic work of indentation approaches were found to give results in good agreement with the literature. The O–P method, despite being influenced by pileup also gives hardness values that are in reasonable agreement with the literature.

For the Al2024, the total work of indentation approach gave the best agreement with the literature values. This is in agreement with the findings of Tuck et al. [13], who found that for ductile materials where significant pileup occurs, the total work of indentation approach always gave good results as compared to the plastic work of indentation technique. Tuck et al. [13] did not fully explain why the total work of indentation approach gives better results than using the plastic work alone, but it may be owing to the subtleties of the fact that elastic recovery tends to affect recovery of indentation depth rather than indentation area, and thus the total work is more representative of the work necessary to create the indentation area. This would make hardness calculated from total work of indentation more directly analogous to hardness values calculated by microhardness or macro-hardness tests.

Conclusions

(1) Al-clad and Al2024-T351 materials have been characterized by nanoindentation. The nanoindentation load–displacement curves have been analyzed to determine the hardnesses and Young's moduli of the samples.

(2) Owing to the relatively high E/σ_y ratio and low strain-hardening exponent of aluminium, pileup occurred at the edges of the indentations. The widely used Oliver and Pharr model does not account for pileup and consequently overestimates hardness and modulus for the Al2024-T351.

(3) AFM imaging was performed to calculate the pileup area, which was found to increase with indentation depth for both Al-Clad and Al2024-T351. The AFM measured pile-up area was found to be overestimated owing to relaxation of material between indentation and imaging, leading to underestimated hardness values.

(4) Work of indentation techniques do not require any calculation of the indentation area and are therefore useful for characterization for soft materials. Hardness values calculated from the total work and plastic work of indentation show good agreement with literature values of the hardness for these materials.

(5) For the soft Al-Clad, where very little elastic recovery is observed, both the total work of indentation and plastic work of indentation methods were found to be effective. For the slightly harder Al 2024-T351 where the material elastically recovers in unloading stage, the total work of indentation technique gave better agreement with literature values.

Acknowledgements Mr I. Norman of Materials Engineering at The Open University is thanked for his help with the experimental work. M. K. Khan is funded by Airbus Deutschland, and Dr D. Furfari is duly acknowledged for his support.

References

1. Oliver WC, Pharr GM (1992) J Mater Res 7:1564
2. Kese KO, Li ZC, Bergman B (2004) J Mater Res 19:3109
3. Beegan D, Chowdhury S, Laugier MT (2005) Surf Coat Technol 192:57
4. Bolshakov A, Pharr GM (1998) J Mater Res 13:1049
5. Kese KO, Li ZC, Bergman B (2005) Mater Sci Eng A404:1
6. Taljat B, Pharr GM (2004) Int J Solids Struct 41:3891
7. Beegan D, Chowdhury S, Laugier MT (2003) Surf Coat Technol 176:124
8. Kese KO, Li ZC (2006) Scripta Mater 55:699
9. Saha R, Nix WD (2001) Mater Sci Eng A319–321:898
10. Tang C, Li Y, Zeng K (2004) Mater Sci Eng A384:215
11. Beegan D, Chowdhury S, Laugier MT (2004) Thin Solid Films 466:167
12. Pharr GM (1998) Mater Sci Eng A253:151
13. Tuck JR, Korsunky AM, Bull SJ, Davidson RI (2001) Surf Coat Technol 137:217
14. Pothapragada RM, Mirshams RA, Vadlakonda S (2005) Mater Res Soc Symp Proc 880E:BB7.9.1
15. Zhou L, Yao Y (2007) Mater Sci Eng A460–461:95
16. Tuck JR, Korsunsky AM, Davidson RI, Bull SJ, Elliott DM (2000) Surf Coat Technol 127:1
17. Stillwell NA, Tabor D (1961) Proc Phys Soc Lond 78:169